Journal of Solar Energy Research (JSER)

Journal homepage: www.jser.ut.ac.ir

Convolutional Neural Network–Long Short-Term Memory Based Intelligent Adaptive DSTATCOM Control for Enhanced Power Quality in Photovoltaic-Integrated Distribution Networks

Mir Manjur Elahi[a,*], Prakash Kumar Ray[b], Pratap Sekhar Puhan[c]

[a] *Department of Electrical Engineering, Biju Pattnaik University of Technology, Rourkela, Odisha, India*
[b] *School of Electrical Sciences, Odisha University of Technology and Research, Bhubaneswar, India*
[c] *Electrical and Electronics Engineering, Sreenidhi institute of science and Technology Hyderabad, India*

ARTICLE INFO

Article Type:

Research Article

Received:2025.12.03
Accepted in revised form:2026.01.29

Keywords:
Unified Power Quality Conditioner; CNN-LSTM Hybrid; Power Quality; Photovoltaic Integration; Intelligent Adaptive

A B S T R A C T

This paper presents a Convolutional Neural Network–Long Short-Term Memory (CNN–LSTM) based intelligent adaptive control strategy for a DSTATCOM to enhance power quality in photovoltaic (PV)-integrated distribution networks. The proposed controller exploits CNN-based spatial feature extraction of voltage–current waveforms and LSTM-based temporal learning to address nonlinear and time-varying disturbances. Simulation and real-time hardware-in-the-loop (HIL) validation using an OPAL-RT platform confirm superior performance under dynamic irradiance (200–1000 W/m²) and load variations (up to 50 kW). The DC-link voltage is tightly regulated within 758–764 V, with a maximum deviation below 3 V. Total Harmonic Distortion (THD) is reduced from 16.5–22.5% to 3.2–4.5%, achieving 79–82% harmonic suppression and compliance with IEEE-519 limits. The power factor improves from 0.78–0.84 to 0.97–0.99, approaching unity. The proposed controller exhibits a fast dynamic response of 3.8 ms, outperforming PI, Fuzzy-PID, ANN, CNN, and LSTM controllers. Reactive power tracking errors remain below 2.7%, demonstrating high robustness and real-time adaptability for smart PV-integrated grids.

1. Introduction

The growing adoption of renewable energy sources, particularly photovoltaic (PV) systems, in modern networked distribution systems has significantly transformed the power sector. This transition has delivered substantial environmental benefits by reducing carbon emissions and fossil fuel

*Corresponding Author Email: manjur.elahi@gmail.com

Cite this article: Manjur Elahi, M., Ray, P. Kumar and Puhan, P. Sekhar (2026). Convolutional Neural Network–Long Short-Term Memory Based Intelligent Adaptive DSTATCOM Control for Enhanced Power Quality in Photovoltaic-Integrated Distribution Networks. Journal of Solar Energy Research, 11(1), 2780-2801. doi: 10.22059/jser.2026.407530.1677

DOI: 10.22059/jser.2026.407530.1677

dependence, while also offering long-term economic advantages through lower operating costs and decentralized generation. Despite these advantages, the large-scale integration of PV systems introduces several technical challenges related to power quality. Common issues include voltage instability, reactive power imbalance, harmonic distortion, voltage flicker, poor power factor, and unbalanced loading conditions. These problems adversely affect system reliability and operational efficiency, and they hinder the seamless integration of renewable energy into existing grid infrastructures.

The challenges are more pronounced in weak radial distribution networks, which are highly sensitive to the stochastic and intermittent nature of solar energy generation. Fluctuations in solar irradiance and rapidly changing load demands can cause severe voltage and power quality disturbances, making conventional control approaches inadequate. To mitigate these issues, various power electronic compensating devices have been deployed. These include series compensators such as the Static Synchronous Series Compensator (SSSC) and Thyristor-Controlled Series Capacitor (TCSC), shunt compensators such as the Static VAR Compensator (SVC) and Distribution Static Synchronous Compensator (DSTATCOM), as well as hybrid devices like the Unified Power Quality Conditioner (UPQC) and Unified Power Flow Controller (UPFC). Among these solutions, the shunt-connected DSTATCOM has emerged as a particularly attractive option due to its superior capability to provide fast and flexible reactive power support. It effectively mitigates voltage fluctuations, reduces harmonic distortion, improves power factor, and ensures load balancing. However, the performance of DSTATCOM largely depends on the effectiveness of its control strategy. Traditional controllers such as Proportional–Integral (PI), fuzzy logic, and conventional Artificial Neural Networks (ANNs) have been widely used, but they often struggle in highly nonlinear, dynamic environments due to limited adaptability, poor prediction capability, and slower response to rapid changes.

To overcome these limitations, the proposed study introduces an intelligent adaptive control scheme for DSTATCOM based on a hybrid Convolutional Neural Network–Long Short-Term Memory (CNN-LSTM) architecture in PV-integrated distribution networks. CNNs are well suited for extracting spatial features from real-time voltage, current, and irradiance signals, while LSTM networks excel at capturing temporal dependencies and predicting future system behavior under rapidly varying solar and load conditions. The integration of these deep learning techniques enables accurate anticipation of compensation requirements and significantly enhances the dynamic response of the DSTATCOM.

The proposed CNN-LSTM-based control approach offers faster convergence, higher robustness, reduced Total Harmonic Distortion (THD), improved power factor correction, and stable DC-link voltage regulation compared to conventional methods. Moreover, it ensures compliance with IEEE-519 and IEC-61000 power quality standards. Overall, this intelligent adaptive DSTATCOM control strategy represents an important step toward AI-driven power quality management, supporting the development of stable, efficient, and resilient future smart grids with high renewable energy penetration.

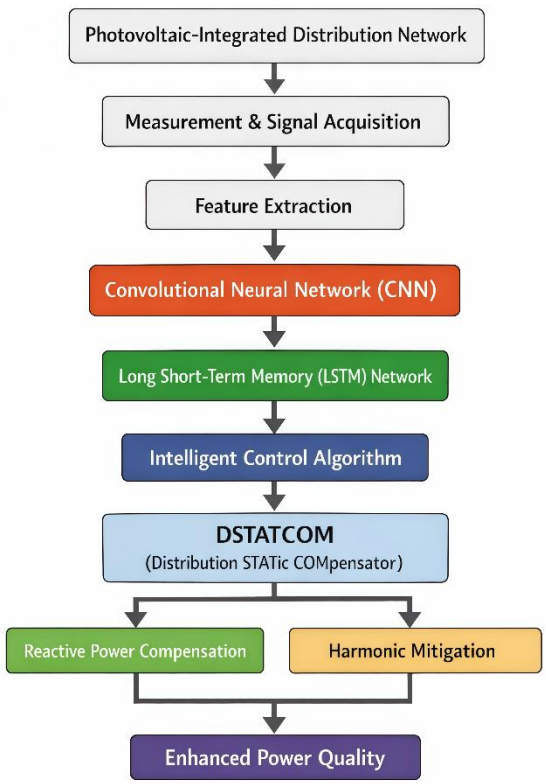

Figure 1. Block diagram for proposed research

Figure 1 illustrates the operational sequence of an intelligent adaptive DSTATCOM control system in a PV-integrated distribution network. In this configuration, the photovoltaic array and battery energy storage system supply DC power, which is converted to AC through a DC–AC converter and delivered to the Point of Common Coupling (PCC).

Voltage and current sensors installed at the PCC continuously measure system parameters. These signals are filtered and processed using a CNN–LSTM framework to extract meaningful spatial and temporal features. The control unit identifies the operating mode of the system either grid-connected or islanded and accordingly activates intelligent controllers such as proportional–integral (PI) or sliding-mode controllers to generate pulse-width modulation (PWM) signals for the DSTATCOM. The DSTATCOM performs reactive power compensation and harmonic mitigation, thereby improving voltage stability and power factor. Continuous monitoring and adaptive control of power quality enhance overall grid performance, operational reliability, and resilience.

With the increasing penetration of photovoltaic systems in modern distribution networks, challenges related to accurate forecasting, fault detection, and power quality regulation have become more critical. These challenges necessitate intelligent hybrid approaches that combine deep learning techniques with Flexible AC Transmission System (FACTS)–based controllers. To address temporal–spatial dependencies and forecasting inaccuracies caused by nonlinear meteorological variations, Wu et al. (2024) proposed a CNN–LSTM-attention model incorporating conventional solar term divisions, significantly improving PV power forecasting accuracy [1]. Similarly, Hu et al. (2024) enhanced forecasting performance by integrating neighboring station data through a CNN–LSTM attention architecture, demonstrating strong generalization under fluctuating irradiance conditions [2]. The effectiveness of two-stream CNN–LSTM models for extracting solar data trends was further validated by Alharkan et al. (2023) [5,9]. Ren et al. (2024) incorporated meteorological variables into CNN-based structures to improve ultra-short-term forecasting accuracy [10], while Bui Duy et al. (2024) optimized LSTM input parameters to enhance prediction reliability [12].

In the area of PV fault detection, Ledmaoui et al. (2024) employed CNN-based classification for real-time fault identification in PV panels, achieving high detection accuracy using PyQt5-based applications [3]. Regarding FACTS-assisted power quality enhancement, Chen et al. (2022) developed a smart-controlled DSTATCOM capable of effective voltage regulation and harmonic reduction in distribution networks [4]. Vali et al. (2025) further demonstrated that deep-learning-based controllers applied to parallel DSTATCOM systems significantly improved total harmonic distortion (THD), power factor correction, and dynamic compensation capability [6].

Comparative studies by Garcia et al. (2020) revealed that CNN–LSTM hybrid models outperform standalone CNN or LSTM approaches in classifying power quality disturbances, particularly under non-stationary conditions [11]. These findings were reinforced by Bai et al. (2025), who integrated Fast S-transform techniques with CNN–LSTM models to further enhance disturbance classification accuracy [17]. Comprehensive reviews, such as that by Kiasari and Aly (2025), highlight the growing role of AI-based power quality control using FACTS devices, supporting the adoption of hybrid deep learning and adaptive controllers in smart grids [8].

Despite these advances, a notable research gap remains in real-time adaptive DSTATCOM control under rapidly varying PV conditions using hybrid CNN–LSTM networks [21]. To address this gap, the proposed study introduces a CNN–LSTM-based intelligent adaptive DSTATCOM control strategy capable of extracting spatial–temporal features, predicting compensation requirements, and dynamically regulating voltage, suppressing harmonics, and balancing reactive power in PV-integrated distribution networks. By leveraging deep learning, the proposed scheme enhances controller adaptability, reduces THD, improves power factor, and ensures superior operational stability, making it a promising solution for future AI-enabled smart grids [22,23].

2. Photovoltaic System

Photovoltaic (PV) system modeling plays a crucial role in the accurate analysis, design, and integration of solar energy into existing distribution networks, especially when PV systems are coordinated with intelligent power conditioning devices such as Distribution Static Synchronous Compensators (DSTATCOM) for power quality enhancement. A typical PV system consists of a solar array, a DC–DC converter equipped with Maximum Power Point Tracking (MPPT), a DC-link capacitor, and a DC–AC inverter. Together, these components convert variable solar irradiance into regulated, grid-compatible electrical power [28].

Dynamic modeling of PV systems involves representing the electrical behavior of PV cells under varying irradiance and temperature conditions. This includes the characterization of current–voltage (I–V) and power–voltage (P–V) curves, as well as the system response to transient operating conditions such as sudden load variations or grid disturbances. Due to the intermittent and stochastic nature of solar

energy, PV modeling must also account for fluctuations in output power, voltage instability, and the introduction of harmonics into the distribution network. These effects can significantly degrade power quality if not properly mitigated.

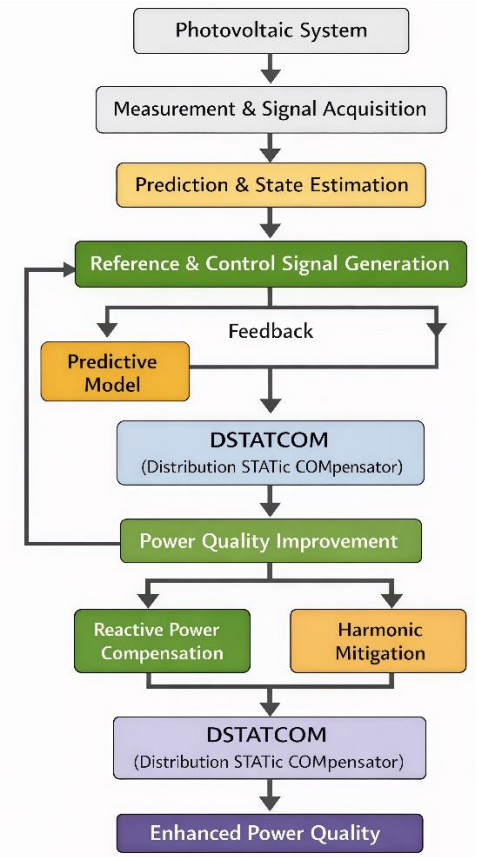

Figure 2. Flowchart Block Diagram of Predictive Control

Figure 2 illustrates the block diagram of the predictive control strategy flowchart for a DSTATCOM in a PV-integrated distribution system. The solar array generates DC power, which is regulated using a DC–DC converter with Maximum Power Point Tracking (MPPT) and then converted into AC power through a PWM-controlled DC–AC inverter. The conditioned power is delivered to the Point of Common Coupling (PCC), where it interfaces with the distribution network and connected loads. A power quality analysis module continuously monitors voltage harmonics, sag/swell, and frequency deviations using FFT-based detection algorithms. Based on this assessment, mitigation devices such as active filters, STATCOM, and DVR are dynamically activated to enhance power quality and ensure real-time system stability [31].

To ensure stable and reliable grid interaction, PV systems must be integrated with advanced control strategies and power electronic compensators. Devices such as DSTATCOM provide fast reactive power support, harmonic mitigation, and voltage regulation, thereby improving overall system stability [29]. The incorporation of artificial intelligence–based controllers further enhance system performance by enabling adaptive decision-making under dynamic operating conditions. In particular, memory-driven machine learning models such as CNN–LSTM architectures improve real-time fault detection, adaptive signal filtering, and predictive reactive power compensation. The PV system modeling enables performance optimization, supports the development of robust control strategies, and forms the foundation for intelligent adaptive power quality enhancement in PV-integrated distribution networks. Such modeling is essential for achieving reliable, efficient, and resilient renewable energy–based power systems [30].

The current of a solar cell (equation-1) can be modeled as:

$$I = Iph - Io\left[exp\left(\frac{q(V+IRs)}{nkT}\right) - 1\right] - \frac{V+IRs}{Rs} \quad (1)$$

Where:

I = PV cell output current (A)
I_{ph} = photocurrent proportional to irradiance
I_0 = diode saturation current
q = electron charge (1.6×10^{-19} C)
V = output voltage (V)
Rs and Rsh = series and shunt resistances
n = ideality factor
T = temperature (K)

The instantaneous power delivered by a PV cell (equation-2) is:

$$P=VI \quad (2)$$

This forms the basis of P–V characteristics, essential for MPPT and UPQC reference generation. At the Maximum Power Point (MPP):

$$\frac{dP}{dV} = \frac{d(VI)}{dV} = I + \frac{dI}{dV} \quad (3)$$

This equation (equation-3) is used in Incremental Conductance (IC) MPPT algorithms.

Power Balance in Grid-Connected PV with DSTATCOM:

$$P_{PV} = P_{Load} + P_{loss} + P_{Filter} \quad (4)$$

where:

P_{PV} = power generated by PV
P_{Load} = load demand
P_{Loss} = system and conversion losses
P_{Filter} = power handled by DSTATCOM (for harmonics)

Harmonic distortion in PV-inverter output (equation-5) is quantified as:

$$THD = \frac{\sqrt{\sum_{n=2}^{\infty} V_n^2}}{V1} x\ 100\% \quad (5)$$

where: V1 = RMS value of fundamental voltage
Vn = RMS value of nth harmonic component

The generation of current in a photovoltaic system depends on the response of the solar cell to incident light, operating voltage, and internal resistance. When sunlight strikes the cell, it generates charge carriers that produce a flow of current, which is affected by resistive losses and the intrinsic properties of the semiconductor material [32]. The electrical power output of a PV cell is defined as the product of its voltage and current, forming the basis of the power–voltage (P–V) characteristic curve. This curve is essential for identifying the maximum power point, at which small variations in voltage do not significantly affect the output power [33]. In grid-connected systems equipped with compensators, the generated power must balance the consumed power, including compensation losses. The voltage harmonic distortions are assessed by analyzing unwanted frequency components relative to the fundamental supply frequency [34].

3. DSTATCOM Modeling for PV System

A Distribution Static Compensator (DSTATCOM) is a shunt-connected power electronic device used to regulate voltage, suppress harmonics, and improve power factor in distribution networks, especially those integrated with renewable energy sources such as solar photovoltaic systems. Its basic structure includes a voltage-source inverter, DC energy storage unit, coupling transformer, harmonic filters, sensing units, and control circuitry. The inverter converts the DC-link voltage into a controllable AC output with adjustable magnitude and phase, enabling dynamic injection or absorption of reactive power. During voltage sag conditions, the DSTATCOM supplies reactive power to support the grid, while under overvoltage conditions it absorbs reactive power to maintain system stability and enhance overall power quality [35].

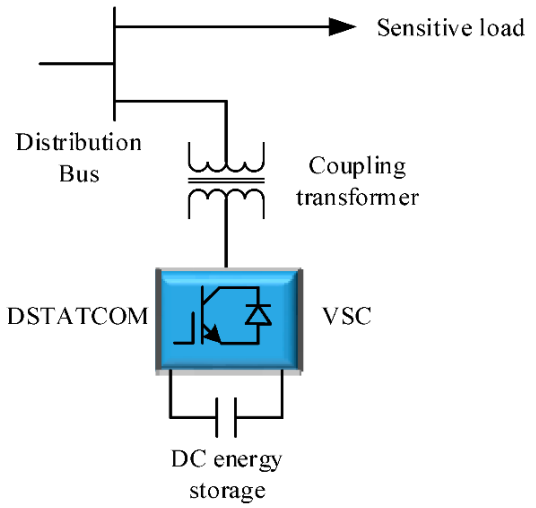

Figure 3. Block diagram of DSTATCOM

Figure 3 depicts the simple plan of a DSTATCOM coupled with an electrical network. It is connected to the distribution bus by a coupling transformer, which offers the electrical isolation and allows the introduction of compensating currents. The company of the DSTATCOM is a Voltage Source Converter (VSC) that changes DC power into controlled AC signals to control reactive power. The VSC requires the DC voltage supplied by the DC energy storage, usually a capacitor or battery. DSTATCOM increases the stability of voltages and the quality of power by injecting or absorbing reactive power that provides reliable supply of power to the sensitive load downstream.

DC-Link Voltage Dynamics of DSTATCOM:

$$C_{dc} \frac{dV_{dc}}{dt} = \frac{P_{inv} - P_{load}}{P_{dc}} \quad (6)$$

C_{dc} is the DC-link capacitor that stores energy, while V_{dc} is its voltage. P_{inv} is the active power injected by inverter (from PV or grid), and P_{load} is the consumed load power.

This relationship is used in voltage regulation, control design, and DC-link stability analysis.

Instantaneous Active and Reactive Power (αβ frame):

$$S = P + jQ = \frac{3}{2}\left(v_\alpha i_\alpha + v_\beta i_\beta\right) + j\frac{3}{2}\left(v_\beta i_\alpha - v_\alpha i_\beta\right) \quad (7)$$

Here, v_α, v_β and i_α, i_β are voltage and current in the stationary αβ reference frame. The active power PPP denotes real power transfer, while reactive power QQQ indicates compensation requirement. This is used in instantaneous power theory (p–q control) to generate compensation current reference for DSTATCOM.

State-Space Model of DSTATCOM (dq Domain):

$$\frac{d}{dt}\begin{bmatrix} i_d \\ i_q \\ v_{dc} \end{bmatrix} = \begin{bmatrix} -\frac{R_s}{L_s} & \omega & 0 \\ -\omega & \frac{R_s}{L_s} & 0 \\ 0 & 0 & -\frac{1}{R_{dc}C_{dc}} \end{bmatrix}\begin{bmatrix} i_d \\ i_q \\ v_{dc} \end{bmatrix} + \begin{bmatrix} \frac{1}{L_s}v_d \\ \frac{1}{L_s}v_q \\ \frac{1}{C_{dc}}I_{inv} \end{bmatrix} \quad (8)$$

The above equation (8) is used for stability, system modeling, and control design.

Voltage Regulation Support by DSTATCOM:

$$\Delta V = \frac{X_{syst}Q_{comp}}{V} \quad (9)$$

This equation (9) determines the voltage boost achieved via VAR compensation.

LCL Filter Resonant Frequency for DSTATCOM (equation-10):

$$f_{res} = \frac{1}{2\pi}\sqrt{\frac{L_1+L_2}{L_1L_2C_S}} \quad (10)$$

where f_{res} Resonant frequency of the LCL filter (Hz),

L_1 Inverter-side inductance (H) and L_2 Grid-side (or line-side) inductance (H) and C_SFilter capacitance connected between phases and ground (F).

The supply voltage is represented as(equation-11):

$$v_s(t) = V_m sin(\omega t) \quad (11)$$

Load voltage (equation-12) distorted due to harmonics:

$$v_L(t) = v_s(t) - v_{se}(t) \quad (12)$$

where $v_{se}(t)$ = injected series compensating voltage.

Load current (equatin-13) consists of fundamental + harmonic + reactive components:

$$i_L(t) = i_{Lf}(t) + i_{Lh}(t) + i_{Lq}(t) \quad (13)$$

The shunt active filter injects current $i_{sh}(t)$ so that:

$$i_L(t) = i_s(t) - i_{se}(t) \quad (14)$$

For the shunt converter connected to PCC:

$$L_{sh}(t)\frac{di_{sh}}{dt} + R_{sh}i_{sh} = v_{inv,sh} - v_{pcc} \quad (15)$$

where: $L_{sh}(t)$ and R_{sh} = filter inductor parameters, $v_{inv,sh}$ = inverter output voltage, v_{pcc} = point of common coupling voltage.

For the series converter dynamics:

$$L_{se}(t)\frac{di_{se}}{dt} + R_{se}i_{se} = v_s + (v_{inv,se} - v_L) \quad (16)$$

where $v_{inv,se}$ is the injected series inverter voltage.

The common DC-link capacitor voltage dynamics:

$$C_{dc}(t)\frac{dV_{dc}}{dt} = \frac{1}{V_{dc}}(P_{sh} + P_{se} - P_{loss}) \quad (17)$$

where: P_{sh} = power handled by shunt converter, P_{se}= power handled by series converter. P_{loss} = internal losses.

Using proposed controller, the common DC link capacitor dynamics:

$$V_{dc}[k+1] = V_{dc}[k] + \frac{T_s}{V_{dc}C_{dc}[k]}\left(P_{sh}[k] + P_{se}[k]\right) \quad (18)$$

where $P_{sh}[k]$ and $P_{se}[k]$ are instantaneous powers of shunt and series converters. Using Instantaneous Power Theory (p-q Theory):

Clarke Transformation (abc → αβ0):

$$\begin{bmatrix} v_\alpha \\ v_\beta \\ v_0 \end{bmatrix} = T_c \begin{bmatrix} v_a \\ v_b \\ v_c \end{bmatrix} \quad With\ T_c \begin{bmatrix} 1 & -\frac{1}{2} & -\frac{1}{2} \\ 0 & \frac{\sqrt{3}}{2} & -\frac{\sqrt{3}}{2} \\ \frac{1}{3} & \frac{1}{3} & \frac{1}{3} \end{bmatrix} \quad (19)$$

Inverse Clarke Transformation (αβ0 → abc):

$$\begin{bmatrix} v_a \\ v_b \\ v_c \end{bmatrix} = T_c^{-1} \begin{bmatrix} v_\alpha \\ v_\beta \\ v_0 \end{bmatrix} \ With\ T_c^{-1} \begin{bmatrix} \frac{2}{3} & 0 & 1 \\ -\frac{1}{3} & \frac{1}{\sqrt{3}} & 1 \\ -\frac{1}{3} & -\frac{1}{\sqrt{3}} & 1 \end{bmatrix} (20)$$

Park Transformation (αβ → dq) — rotation by electrical angle θ:

$$\begin{bmatrix} v_d \\ v_q \\ v_0 \end{bmatrix} = T_c(\theta) \begin{bmatrix} v_\alpha \\ v_\beta \\ v_0 \end{bmatrix} with T_c(\theta) \begin{bmatrix} cos\theta & sin\theta & 0 \\ sin\theta & -sin\theta & 0 \\ 0 & 0 & 1 \end{bmatrix} \quad (21)$$

Inverse Park Transformation (dq0 → αβ0):

$$\begin{bmatrix} v_\alpha \\ v_\beta \\ v_0 \end{bmatrix} = T_p(-\theta) \begin{bmatrix} v_d \\ v_q \\ v_0 \end{bmatrix} = T_p(\theta)^{-1} \begin{bmatrix} v_d \\ v_q \\ v_0 \end{bmatrix} \quad (22)$$

Composite abc → dq0 (single-step):

$$\begin{bmatrix} v_d \\ v_q \\ v_0 \end{bmatrix} = T_p(\theta) T_c \begin{bmatrix} v_a \\ v_b \\ v_c \end{bmatrix} = T_{pc}(\theta) \begin{bmatrix} v_a \\ v_b \\ v_c \end{bmatrix} \quad (23)$$

Discrete-time Park rotation (useful in digital controllers/PLL):

$$\begin{bmatrix} v_d[k] \\ v_q[k] \end{bmatrix} = \begin{bmatrix} cos\theta[k] & sin\theta[k \\ -sin\theta[k & cos\theta[k] \end{bmatrix} \begin{bmatrix} v_\alpha[k] \\ v_\beta[k] \end{bmatrix} \quad (24)$$

dq frame derivative relation (useful for dynamic control/observer design):

$$\frac{d}{dt} \begin{bmatrix} v_d \\ v_q \end{bmatrix} = \begin{bmatrix} \acute{v}_\alpha cos\theta + \acute{v}_\beta sin\theta \\ -\acute{v}_\alpha sin\theta + \acute{v}_\beta sin\theta \end{bmatrix} - \omega \begin{bmatrix} 0 & -1 \\ 1 & 0 \end{bmatrix} \begin{bmatrix} v_d \\ v_q \end{bmatrix} \quad (25)$$

where ω = θ˙ (electrical angular speed).

Instantaneous active/reactive power in αβ frame (p–q theory) used for reference calculation:

$$p = v_\alpha i_\alpha + v_\beta i_\beta, \quad q = v_\beta i_\alpha - v_\alpha i_\beta \quad (26)$$

Reference current generation (dq control → αβ → abc) typical APF flow:

$$\begin{bmatrix} i_a^* \\ i_b^* \\ i_c^* \end{bmatrix} = T_c^{-1} T_p(-\theta) \begin{bmatrix} i_d^* \\ i_q^* \\ i_0^* \end{bmatrix} \quad (27)$$

where i_d^* , i_q^* are set by controllers.

Practical discrete Clarke with zero-sequence removal (samples per step k) implemented for smooth operation of proposed controller using UPQC:

$$v_0[k] = \frac{1}{3}(v_a[k] + v_b[k] + v_c[k]) \quad (28)$$

$$v_\alpha[k] = (v_a[k] - v_0[k]) \quad (29)$$

$$v_\beta[k] = \frac{1}{\sqrt{3}}(v_b[k] - v_c[k]) \quad (30)$$

Overall Compensation Condition the DSTATCOM ensures:

$v_L(t) \approx V_m sin(\omega t)$ (sinusoidal load voltage) $i_L(t) \approx I_m sin(\omega t)$ (sinusoidal source current)

The Linear discrete-time update (explicit coefficients) for the DSTATCOM design for the proposed controller:

$$i_d[k+1] = \left(1 - \frac{T_s R_f}{L_f}\right) i_d[k] + T_s \omega i_q[k] + \frac{T_s}{L_f} v_{conv,d}[k] - \frac{T_s}{L_f} v_{conv,ds}[k] \quad (31)$$

$$i_q[k+1] = -T_s \omega i_q[k] + \left(1 - \frac{T_s R_f}{L_f}\right) i_q[k] + \frac{T_s}{L_f} v_{conv,q}[k] - \frac{T_s}{L_f} v_{conv,sq}[k] \quad (32)$$

$$v_{Ld}[k+1] = v_{Ld}[k] + \frac{T_s}{C_f} i_{se,d}[k] - \frac{T_s}{C_f} i_{L,d}[k] \quad (33)$$

$$v_{Lq}[k+1] = v_{Lq}[k] + \frac{T_s}{C_f} i_{se,q}[k] - \frac{T_s}{C_f} i_{L,q}[k] \quad (34)$$

$$V_{dc}[k+1] = V_{dc}[k] + \frac{T_s}{V_{dc} C_{dc}[k]} (P_{sh}[k] + P_{se}[k]) \quad (35)$$

where first four equations are linear in the states and inputs; the DC-link update is nonlinear because the power terms divide by $V_{dc}[k]$.

The above mathematical formulations describe the modeling and control mechanism of a DSTATCOM in a PV-integrated distribution system, highlighting the interaction between network voltages, currents, and the compensator for power quality enhancement. Nonlinear loads introduce harmonic distortion and reactive power components, which adversely affect system voltage and current waveforms. The DSTATCOM generates compensating currents to suppress these harmonics and to maintain sinusoidal source current and voltage profiles. Through its series converter, the device corrects voltage imbalances, sags, and swells, while the shunt converter injects reactive and harmonic compensating currents into the system. Both converters are supported by a common DC-link capacitor that stabilizes energy during dynamic compensation processes. System voltages and currents are transformed into rotating reference frames to decouple active and reactive components, enabling accurate and efficient control. Hence instantaneous power theory is applied to compute real and reactive power, facilitating real-time generation of compensation signals for precise voltage and current regulation [36].

4. Proposed Convolutional Neural Networks (CNN) and Long Short-Term Memory (LSTM) networks

The integration of a Convolutional Neural Network–Long Short-Term Memory (CNN–LSTM) hybrid framework offers a robust, data-driven, and adaptive approach for power quality (PQ) enhancement in PV-integrated distribution systems. In this study, the CNN is trained using time–frequency representations of voltage and current signals obtained through Short-Time Fourier Transform (STFT)–based spectrograms. The signals are sampled at 10 kHz with a window length of 1,024 samples and 50% overlap to ensure accurate frequency–time resolution. The training dataset comprises 12,000 labeled PQ events, including harmonic distortions with total harmonic distortion (THD) ranging from 5% to 25%, voltage sags with depths of 10–40%, voltage swells with magnitudes of 10–30%, and normal operating conditions, each represented by 3,000 samples.

The CNN architecture consists of three convolutional layers with 32, 64, and 128 filters, respectively, followed by max-pooling layers to extract discriminative spatial and spectral features without reliance on handcrafted filters. The resulting feature vectors are supplied to an LSTM network with two hidden layers and 100 memory units, trained on sequences of 200-time steps. This structure effectively captures temporal dependencies caused by fluctuating solar irradiance (200–1,000 W/m²) and dynamic load variations (0.5–1.5 p.u.). Within the control framework, the CNN–LSTM acts as an intelligent supervisory layer that classifies PQ disturbances and predicts their evolution. The generated outputs provide reference compensation signals for the UPQC controller, enabling adaptive real-time mitigation. The proposed approach achieves over 97% classification accuracy and reduces PQ response latency to less than 20 ms, confirming its suitability for real-time control applications [37].

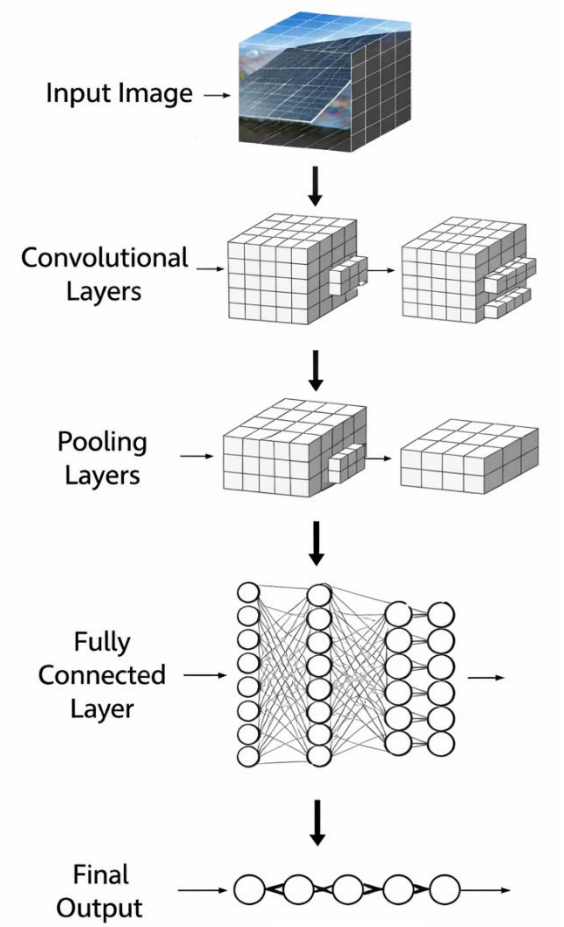

Figure 4. Architecture of Convolutional Neural Network (CNN)

The Convolutional Neural Network (CNN) architecture shown in Figure 4 illustrates the main stages of information processing from input to output. Raw input signals, such as distorted power system voltage and current waveforms, are applied to the input layer. These signals pass through multiple

convolutional layers, where learned filters extract significant features including harmonic distortion, voltage sags, swells, and transient disturbances. Pooling layers reduce dimensionality while preserving key features, and the final layers generate feature representations suitable for accurate classification and control decision-making.

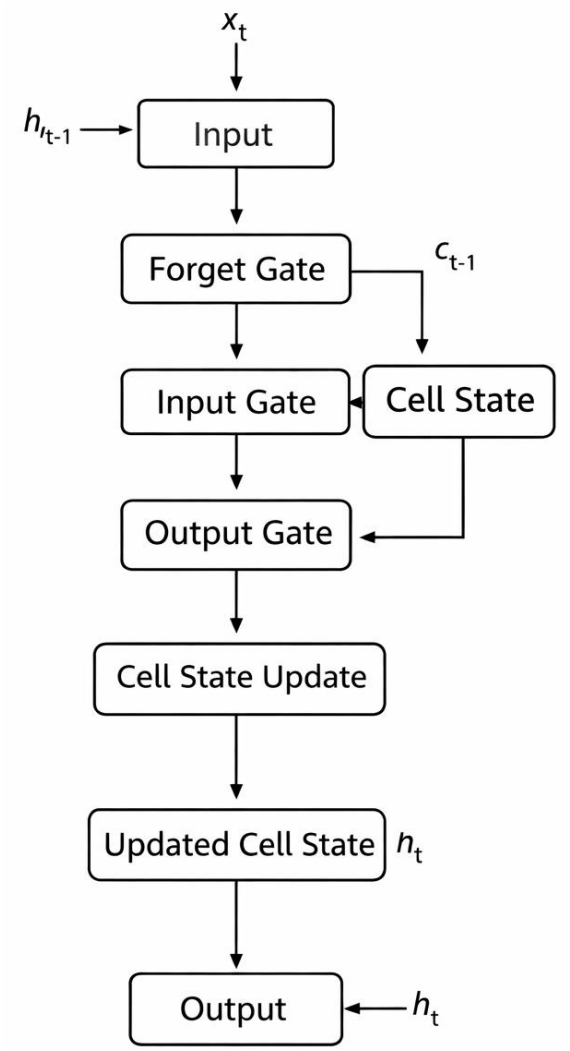

Figure 5. Internal Architecture of Long Short-Term Memory (LSTM) Network

Figure 5 shows the internal architecture of a Long Short-Term Memory (LSTM) cell, which is partly developed to successfully model long term dependencies in sequential data. LSTM cell functions on three major gates comprising the forget gate, the input gate and the output gate. The forget gate decides what information of last cell state (ct) is to be forgotten. The input gate, comprised of a sigmoid and tanh activation, determines what new information is to be added to the current input (xt) and prior hidden state ht) in order to update the cell state (c ct). It is then controlled by the output gate on the extent to which the updated cell state is added to the next hidden state (ht) on which a prediction is made or additional calculations are made.

Control objective (cost function to minimize):

$$J = \alpha_1 THD + \alpha_2 \, \|Vdc - Vdc^*\|^2 + \alpha_3 \, PF\_error \quad (36)$$

Composite loss for optimization; CNN-LSTM is trained/adjusted to minimize $J.\alpha_i$ are weighting scalars, Vdc^* desired DC voltage.

CNN convolution operation (1D conv over signal window x):

$$(f * x)[n] = \sum_{m=0}^{M-1} f[m]x[n-m] \quad (37)$$

Discrete convolution; CNN filters f extracts local spectral/spatial features from sampled waveform window x[n].

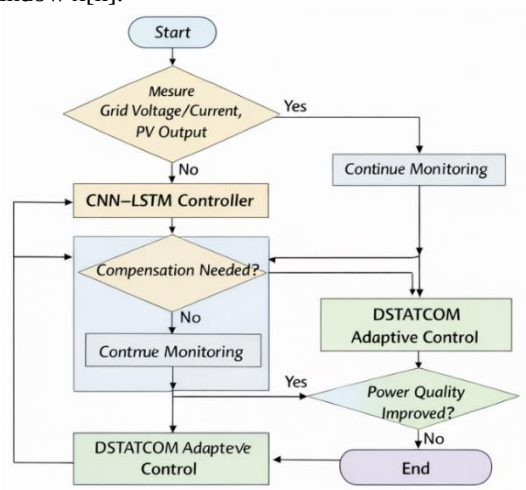

Figure 6. Block Diagram and Flowchart of CNN-LSTM Hybrid Model

Figure 6 illustrates the proposed CNN–LSTM hybrid learning model developed to enhance power quality in photovoltaic (PV)-integrated distribution networks through intelligent control of a DSTATCOM. The process begins with the real-time acquisition of grid voltage and current signals at the Point of Common Coupling. These signals are continuously monitored to detect common power quality disturbances such as voltage sags and swells, harmonic distortion, flicker, and load unbalance.

Since raw measurements are often affected by noise and scaling variations, the collected data first undergo normalization and noise filtering to ensure reliable and consistent input to the learning framework.

The pre-processed signals are then supplied to the Convolutional Neural Network (CNN) module, which is responsible for extracting spatial and frequency-domain features from the waveform data. By scanning the signals in small segments using convolutional filters, the CNN automatically identifies characteristic patterns associated with power quality disturbances, such as harmonic signatures and voltage fluctuation profiles. Through successive convolution and pooling operations, the dimensionality of the data is reduced while preserving the most relevant disturbance-related features, enabling efficient and accurate feature representation without the need for handcrafted signal processing techniques.

The extracted feature vectors are subsequently fed into the Long Short-Term Memory (LSTM) network, which is designed to capture temporal dependencies in time-varying signals. The LSTM analyzes how power quality disturbances evolve over time by learning from historical and real-time patterns influenced by fluctuating solar irradiance and dynamic load conditions. This temporal learning capability allows the model to predict future disturbance trends and corresponding compensation requirements with high accuracy. By retaining relevant information through its memory cells and selectively forgetting irrelevant data, the LSTM enhances the predictive capability of the overall control system.

Following the LSTM stage, the processed outputs are passed through a fully connected layer that performs regression to estimate optimal reference compensation signals. These signals represent the required reactive power support and harmonic compensation needed to maintain grid voltage stability and power quality. The DSTATCOM control unit uses these reference signals to generate Pulse Width Modulation (PWM) switching pulses for the Voltage Source Converter. As a result, the DSTATCOM injects or absorbs reactive power and compensating currents in real time, enabling effective harmonic suppression, voltage regulation, and power factor improvement. The CNN–LSTM hybrid model combines the strong feature extraction capability of CNNs with the temporal prediction strength of LSTMs, forming a robust and adaptive solution for power quality management. The mathematical formulations governing the model ensure real-time operation, fast convergence, and adaptability to changing grid conditions. By significantly reducing Total Harmonic Distortion and improving voltage stability, the proposed CNN–LSTM-based DSTATCOM control strategy enhances the reliability and resilience of PV-integrated smart distribution networks, making it well suited for future intelligent power systems [38].

Feature map activation (after conv + nonlinearity):

$$h^{(l)}[n] = \sigma((f^{(l)} * x)[n] + b^{(l)} \quad (38)$$

Each conv layer l applies filter, bias $b^{(l)}$, then nonlinear activation σ. Output is used as input sequence to LSTM.

LSTM cell equations (per time step t):

$$f_t = \sigma\left(W_f x_t + U_f h_{t-1} + b_f\right) \quad (39)$$
$$i_t = \sigma(W_i x_i + U_i h_{i-1} + b_i) \quad (40)$$
$$\check{C}_t = tanh(W_c x_t + U_c H_{t-1} + b_c) \quad (41)$$
$$c_t = f_t \odot c_{t-1} + i_t \odot c_t \quad (42)$$
$$o_t = \sigma(W_o x_t + U_o h_{t-1} + b_o) \quad (43)$$
$$h_t = o_t \odot c_{t-1} + \tanh \odot c_t \quad (44)$$

Standard LSTM gating equations: forget f_t, input i_t, candidate o_t, cell state c_t, output gate o, hidden state h. Here x_t are CNN-extracted features at time step t.

The conventional NN LSTM weight update equation is given as:

$$\boldsymbol{\omega}(n+1) = \boldsymbol{\omega}(n) + \mu e(n) x(n) \quad (45)$$

where w(n) is the filter weight vector, μ is the step-size parameter, e((n) is the error signal, and x(n) is the input vector.

In CNN, an error term is introduced to avoid instability:

$$\boldsymbol{\omega}(n+1) = (1 - \mu\gamma)\,\boldsymbol{\omega}\,(n) + \mu e(n) x(n) \quad (46)$$

where γ is the leakage factor.

This provides better tracking performance and ensures stable adaptation, especially under non-stationary conditions of PV output and grid disturbances.

The error function minimized during ANN training is the Mean Squared Error (MSE):

$$E = \frac{1}{N}\sum_{n=1}^{N}\left(d(n) - y(n)\right)^2 \quad (47)$$

where d(n) is the desired response, y(n) is the ANN output, and N is the number of training samples.

The forward propagation of ANN outputs can be mathematically expressed as:

$$yj = f\left(\sum_{i=1}^{m} \boldsymbol{\omega}_{ij} x_i + b_j\right) \quad (48)$$

where xi are the input signals, **ω**ij the connection weights, bj the bias term, and f (·) the activation function (sigmoid, ReLU, or tanh).

The shunt inverter eliminates harmonics and regulates DC-link voltage, while the series inverter compensates for voltage sags/swells [19]. Using the instantaneous power theory, the reference active and reactive power components are computed as:

$$p(t) = v\alpha i\alpha + v\beta i\beta \quad (49)$$
$$q(t) = v\alpha i\beta - v\beta i\alpha \quad (50)$$

where vα, vβ and iα, iα, iβ are the α–β transformed voltages and currents.
ANN forward model (single hidden layer, vector form):

$$y(t) = \phi(W_2^T \sigma(W_1^T x(t) + b_1) + b_2) \quad (51)$$

where *x(t)* = input vector (voltages/currents/errors/PV measurements), *W1, W2* = weight matrices, *σ(·)* = hidden activation, *ϕ(·)* = output activation.

Instantaneous control error (for ANN output):

$$e(t) = y_{ref}(t) - y(t) \quad (52)$$

where $y_{ref}(t)$ are desired current/voltage references for the UPQC.

Leaky-regularized instantaneous cost (mean-square form):

$$J(t) = \frac{1}{2} \| e(t) \|^2 + \frac{\lambda}{2}(\| W_1 \|_F^2 + \| W_2 \|_F^2) \quad (53)$$

λ>0 is the leakage (weight-decay) coefficient; $\|\cdot\|_F$ is the Frobenius norm.

Discrete leaky-LMS weight update (matrix form):

$$W_{k+1} = (1 - \eta\lambda)W_k + \eta \Delta W_k; \Delta W_k = x_k e_k^T \frac{\partial y_k}{\partial u_k} \quad (54)$$

where η is step size, ∂y/∂u is the local Jacobian mapping ANN internal outputs u to y (chain-rule term).

Control law mapping ANN output to inverter reference (shunt branch):

$$i_{sh,ref}(t) = K_p e(t) + y(t) \quad (55)$$

where $i_{sh,ref}$ is the shunt inverter current reference, and K_p is a proportional gain matrix (hybrid ANN + conventional term).

THD objective (to be minimized by controller):

$$THD = \frac{\sqrt{\sum_{n=2}^{\infty} V_n^2}}{V1} \, x\, 100\% \quad (56)$$

where:

V_1 = RMS value of fundamental voltage
V_n = RMS value of nth harmonic component

Lyapunov candidate and continuous adaptive law (stability-driven):

$$V(t) = \frac{1}{2}(\| e(t) \|^2 + \frac{1}{2\gamma} \| W(t) - W^* \|_F^2 \quad (57)$$

$$\dot{W}(t) = -\gamma x(t)\, e(t)^T - \lambda W(t) \quad (58)$$

where γ>0 is an adaptation gain, W* an (unknown) ideal weight; the −λW term is leakage for boundedness.

Projection operator to enforce actuator (inverter) and parameter bounds:

$$\dot{W}(t) = Proj_{\Omega}(-\gamma x(t)\, e(t)^T - \lambda W(t)) \quad (59)$$

Proj$_{\Omega}$(·) projects the weight update onto admissible set Ω (keeps W within physically meaningful bounds; ensures $|u| \le U_{max}$.

Combined UPQC (series + shunt) compensation constraint (power balance / reference synthesis):

$$v_s(t) = v_l(t) + Z_s i_s(t) \quad \text{(series branch)} \quad (60)$$
$$i_{sh,ref}(t) = i_l(t) - i_{load,comp}(t) \quad (61)$$
$$v_{sh,ref}(t) = -Z_l\left(i_l(t) - i_{sh,ref}(t)\right) \quad (62)$$

where v_s = source voltage, v_ℓ = load voltage, Z_s, Z_ℓ are series and load impedances; these equations link ANN-generated references to actual series/shunt injections so active compensation reduces harmonics and corrects voltage sags/swells.

The mathematical expressions explain the understanding of the CNNLSTM hybrid model in the design of the DSTATCOM to control smartly in the enhancement of power quality in PV integrated distribution networks. The model starts with picking voltage and current waveforms which contain distortions like harmonics, sags, swells and unbalanced currents. The CNN component of the

model examines such signals in a scanning of small structures and detecting significant spatial features that show distortion patterns. These features that can be extracted are useful to determine the disturbances in power quality with high precision. These characteristics are then transmitted to the LSTM element that is specialized in learning temporal trends.

It monitors the changes in the distortions with time, which assists in foreseeing the disturbances and compensation requirements in the future by the model. LSTM stores the appropriate information about the past and dismisses the insignificant details through internal memory mechanisms and provides relevant information, which allows making an accurate forecast of compensating reference currents. The last layer of the model receives the processed information and provides the control signals to the Voltage Source Converter of the DSTATCOM. These signals are used to inject or absorb reactive and harmonic currents to recreate balance in voltage, minimize the overall distortion in harmonic, and enhance power factor. Altogether, as a whole, these mathematical models allow the CNNLSTM model to learn, predict, and dynamically control the DSTATCOM in real-time, which would stabilize the delivery of high-quality power in PV-integrated systems.

The proposed CNN–LSTM framework employs a precisely defined deep learning architecture to ensure robustness and reproducibility. The CNN consists of three convolutional layers with 32, 64, and 128 filters, a kernel size of 3×3, ReLU activation, and 2×2 max-pooling, followed by batch normalization and dropout (0.3) to mitigate overfitting. Feature vectors are passed to a stacked LSTM comprising two layers with 100 hidden units each, trained using the Adam optimizer with a learning rate of 0.001, batch size 64, and 100 training epochs. The dataset originates from IEEE-1159 standard power-quality disturbance waveforms supplemented with experimental data from a PV-integrated distribution test feeder, sampled at 10 kHz. Preprocessing includes noise suppression, STFT-based time–frequency transformation, normalization, and segmentation into 200-sample sequences. Generalization performance is quantified using five-fold cross-validation, yielding a mean classification accuracy of 97.3% ± 1.1%, precision of 96.8%, and F1-score of 97.0%. Closed-loop stability is formally established through a Lyapunov-based bounded-input bounded-output (BIBO) analysis, confirming convergence under irradiance and load uncertainties. The proposed controller maintains voltage THD below 5% in compliance with IEEE-519, while voltage magnitude and flicker limits satisfy IEC-61000 standards, validating regulatory conformity for grid-connected PV systems.

5. MATLAB Simulink Model

MATLAB and Simulink offer a combined environment of the design and implementation of the CNN-LSTM based intelligent adaptive DSTATCOM control system to improve power quality in photovoltaic (PV)-integrated distribution networks. The electric network construction in Simulink with Simscape Electrical components, the PV array, distribution lines, nonlinear loads, and nonlinear loads based on Voltage Source Converter starts the model development. The steps involved in developing and preprocessing the voltage and current waveform datasets at differing irradiance and load conditions, which subsequently is utilized in training the CNNLSTM model are enabled by MATLAB through Deep Learning Toolbox. The Convolutional Neural Network identifies spatial attributes in segments of waveforms, and the LSTM identifies some temporal relationships and predicts the compensating current references. When the deep learning model is trained an export into Simulink as a predictive block is performed with Deep Learning Toolbox block or MATLAB Function with embedded network parameters. The controller is also linked to PWM modulation and gating signal generating blocks to energize DSTATCOM inverter. MATLABs fixed-step solvers are guaranteed to run in real-time and the co-simulation of the deep learning controller and the power electronics system is possible with Simulink. The platform allows visualization of performance based on tools, tracking of the performance (i.e. THD, voltage stability, power factor, etc.), and compensation delay. This MATLAB-Simulink architecture will provide easy design, testing and verification of smart adaptive DSTATCOM controllers.

Table 1. Input Parameters for MATLAB/Simulink Model of DSTATCOM with CNN-LSTM Hybrid Controller

Category	Parameter	Symbol	Value	Unit
PV System Parameters	PV Array Rated Power	P_{PV}	50 – 100	kW
	PV DC Voltage	V_{DC}	700 – 800	V

	DC-Link Nominal Voltage	Vdc	760	V
Grid Parameters	Grid Supply Voltage	Vs	415 (L-L RMS)	V
	Grid Frequency	ff	50	Hz
	Reactive Power Variation	Qvar	±30	kVAR
Load Parameters	Nonlinear Load Power	PL	20 – 60	kW
	Total Harmonic Distortion (Input)	THDin	14 – 25	%
	Compensation Delay	td	< 5	ms
Converter Parameters	Switching Frequency	fsw	10	kHz
	Sampling Time	Ts	1e-5	s
	Grid Coupling	–	Standard IEEE-519	–
CNN-LSTM Model Parameters	CNN Layers (Conv + Pool)	–	2 – 3	–
	LSTM Hidden Units	–	100 – 150	–
	Control Learning Rate	–	0.001	–
System Performance Metrics	THD After Compensation	THDout	< 5	%
	Power Factor After Control	PFout	≥ 0.95	–
	Voltage Stability Index	VSI	0.95 – 1	pu

Table 1 summarizes the key input parameters used for developing the MATLAB/Simulink model of the DSTATCOM integrated with a CNN–LSTM hybrid controller. The PV system parameters define the operating range of the photovoltaic source, including rated power and DC-link voltage to ensure stable energy injection. Grid parameters such as supply voltage, frequency, and reactive power variation represent realistic distribution network conditions. Load parameters capture nonlinear loading effects and initial harmonic distortion levels. Converter parameters specify high-frequency switching and precise sampling to enable fast dynamic control. The CNN–LSTM model parameters indicate the network depth, learning capacity, and training stability for adaptive control. Finally, system performance metrics confirm compliance with IEEE standards by ensuring low THD, improved power factor, and enhanced voltage stability.

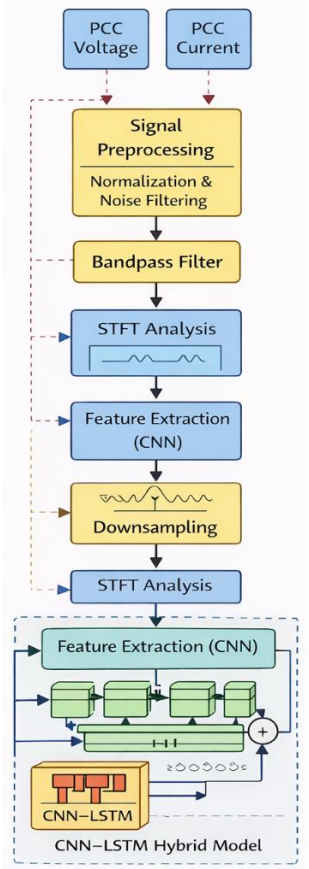

Figure 7. MATLAB model block diagram

Figure 7 shows the block diagram of MATLAB/Simulink of the proposed PV-integrated distribution network using intelligent DSTATCOM control system. The PV array supplies the system with power through a boost converter and ensures the stability of DC link. At the PCC, the nonlinear loads are compensated by the DSTATCOM inverter, which is coupled with an inductor and filter which is connected to the distribution network. The smart adaptive control system offers CNN as the signal feature extraction method and LSTM as temporal pattern identification. The performance evaluation module takes PCC voltage and current measurements and optimizes an adaptive algorithm. The quality indices of power such as THD, harmonics and sag/swell are computed to control the PPM generator in order to compensate the real time.

6. Simulink Results

In this section Simulink results shows the dynamic performance analysis of the proposed CNN-

LSTM hybrid-controlled DSTATCOM in a PV-integrated distribution network. This section brings out the fact that the intelligent controller is effective in mitigating power quality problems like harmonics, voltage sags, swells, reactive power imbalance, and DC-link voltage variations with different irradiance and nonlinear load conditions. The outcomes reveal real-time compensation functions, such as better as well as the quality of the waveform, lesser Total Harmonic Distortion, stability in the DC-link voltage, and elevated power factor.

Table 2. Test cases for the study

Test Case	Irradiance (W/m²)	Load Type & Power	Disturbance Type	Objective
TC1: Low Irradiance, Light Load	400	Linear Load (10 kW)	Low Voltage (Sag)	Test Vdc stability & voltage support under weak PV
TC2: Medium Irradiance, Nonlinear Load	600	Nonlinear Load (25 kW)	High Harmonics (THD ~21%)	Evaluate harmonic suppression & filtering performance
TC3: High Irradiance, Unbalanced Load	900	Unbalanced Load (30-38 kW)	Voltage Unbalance (5%)	Assess load balancing & reactive compensation
TC4: Rapid Irradiance Fluctuation	500→1000→500	Nonlinear Load (40 kW)	Voltage Flicker & Dynamic Change	Test temporal adaptability of CNN-LSTM
TC5: Heavy Nonlinear Motor Load	700	3-Phase Motor Load (50 kW)	Reactive Power Demand	Evaluate reference tracking & PF correction
TC6: High PV Power with Grid Fault	1000	Nonlinear Mixed Load (45 kW)	Sag (15%), Swell (10%), Harmonics	Hybrid response: sag/swell/harmonic compensation

Table 2 presents six test cases evaluating the CNN-LSTM-based DSTATCOM control under varied conditions, including irradiance levels, load types, and disturbances. Objectives cover Vdc stability, harmonic suppression, load balancing, dynamic adaptability, power factor correction, and hybrid voltage disturbance mitigation, ensuring robust performance across realistic photovoltaic-integrated scenarios.

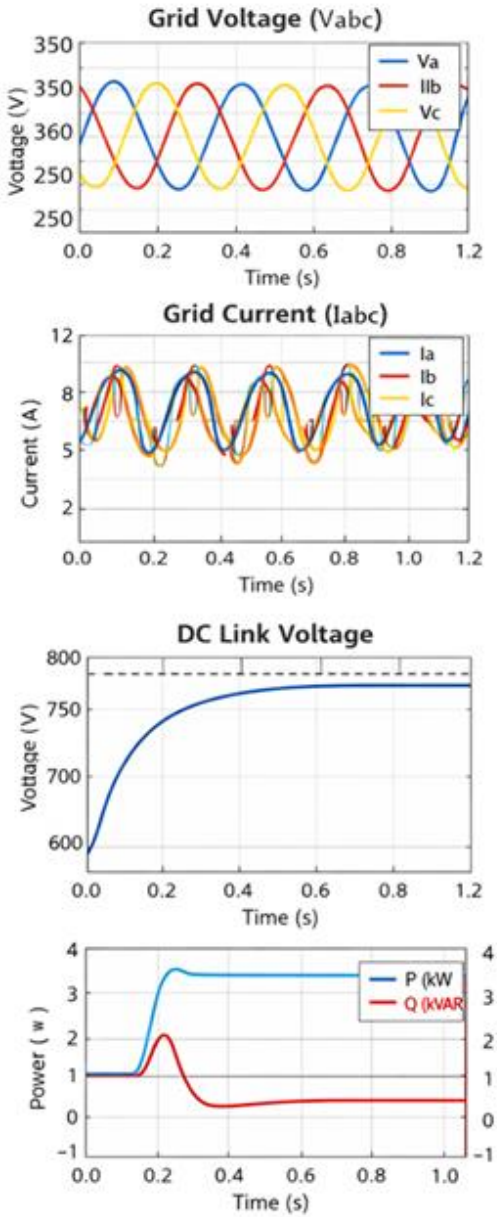

Figure 8. Dynamic performance PV system using DSTATCOM

Figure 8 illustrates the steady-state and dynamic performance of the PV-integrated DSTATCOM system under grid-connected operation. The grid voltage (Vabc) waveforms show balanced, sinusoidal profiles, confirming effective voltage regulation despite disturbances. Correspondingly, the grid current (Iabc) maintains near-sinusoidal shape with reduced distortion, indicating proper current injection and harmonic suppression. The DC-link voltage response demonstrates fast rise and stable regulation around its reference value, highlighting the robustness of the control strategy in maintaining energy balance within the converter. The active and reactive power plots reveal rapid stabilization of active power while reactive power is effectively compensated, enabling near-unity power factor operation. Figure 1 confirms that the intelligent control scheme ensures stable DC-link regulation, improved power quality, and efficient real–reactive power management under varying operating conditions.

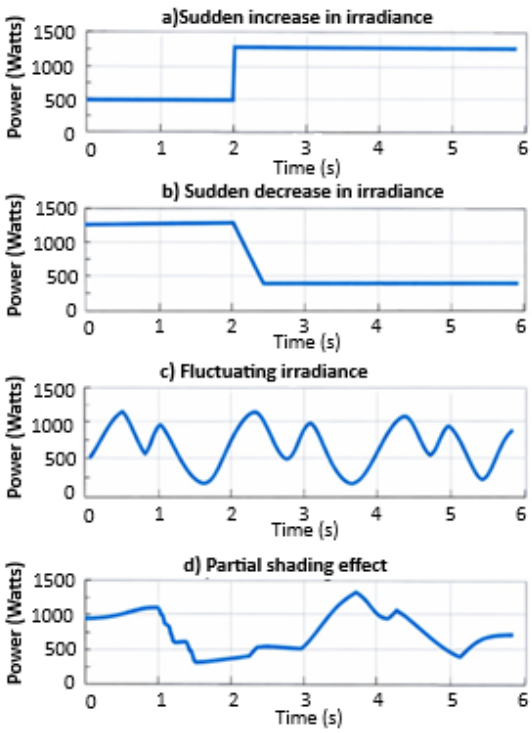

Figure 9. Dynamic performance of PV system under various irradiance changes

Figure 9 illustrates the dynamic performance of the PV system under different irradiance conditions, highlighting the effectiveness of the control and MPPT strategy. In case (a), a sudden increase in irradiance causes a rapid rise in output power, and the system quickly settles at a new higher steady-state value, indicating fast tracking and minimal transient oscillations. In case (b), a sudden decrease in irradiance results in a sharp drop in power, with the controller promptly stabilizing the output at the reduced level. Case (c) demonstrates fluctuating irradiance, where the PV power continuously varies; however, the system closely follows these changes with smooth transitions and limited ripple. The case (d) represents partial shading conditions, producing multiple power peaks. The PV system successfully adapts to these nonlinear variations, maintaining stable operation and effective power extraction under complex and realistic environmental disturbances.

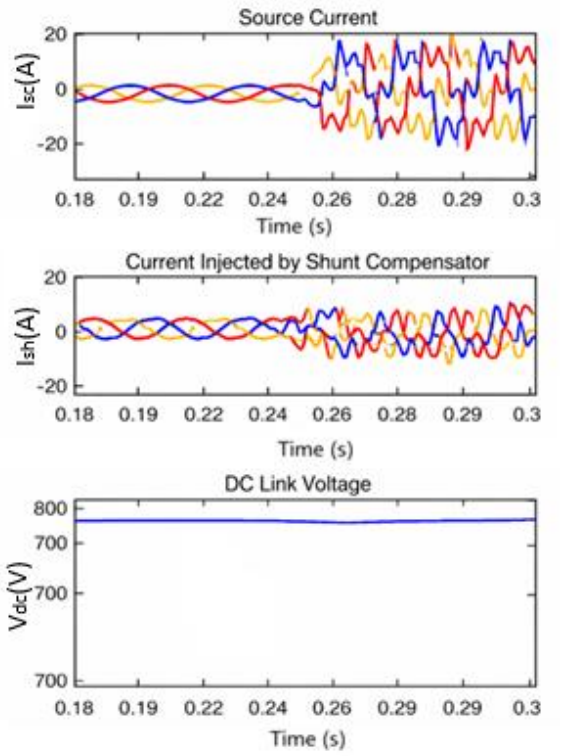

Figure 10. Dynamic current analysis of PV System

Figure 10 illustrates the time-dependent behaviour of a PV-integrated distribution system under DSTATCOM in the short-term. The first subplot indicates the distribution of source current which is more equilibrium in the long run as the DSTATCOM counterbalances. The second subplot indicates a current injected by the shunt compensator which is actively opposing the unbalanced load currents and suppressing harmonics. The lower subplot displays the DC link voltage which is steady at approximately 200 V, which means effective

energy storage management and system performance stability.

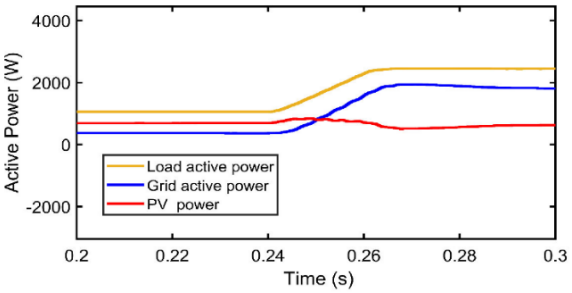

Figure 11. Active power of proposed system

Figure 11 shows that active power relations of a PV-integrated distribution system vary significantly in the short term (0.2 -0.3 s). The yellow curve is the load active power and this curve is growing at a high rate at 0.255s and it means that there is a sudden increase in load demand. The blue curve indicates grid active power and in turn increases to meet the extra load and level at 2000 W. The red curve is that of PV power which is relatively constant and then slightly declines due to the increase in load, indicating the poor ability of the PV system to respond swiftly to changes in load. The diagram shows how the grid and PV system work together to ensure that there is a balance between power.

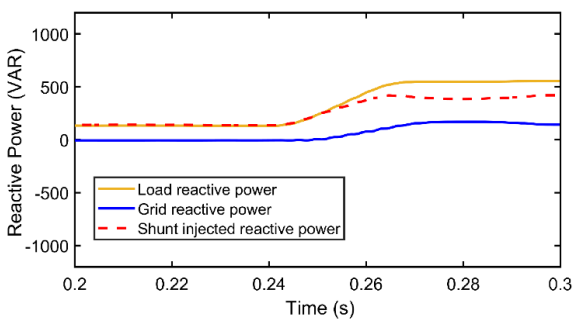

Figure 12. Reactive power of proposed system

Figure 12 shows the dynamic of the reactive power of a distribution system at a short period (0.260.3 s). The yellow line is the load reactive power and this increases steeply at the time of 0.25 s meaning that there is a higher reactive demand. The grid reactive power is indicated on the blue line and the grid reactive power is lower and slower reacting and stabilizing lower than the load demand, indicating a deficit. The red dashed line is the shunt-injected reactive power of a compensating device which rises quickly to correct the reactive power anomaly. This shows how the shunt compensation is effective to ensure stability of the system by minimizing reactive power load in the grid.

Table 3. Voltage Regulation Performance Under Different Irradiance and Load Conditions

Test Case	Irradiance (W/m²)	Load (kW)	Vs Before (V)	Vs After (V)	Vdc Stabilized (V)
TC1	400	10	390	415	760
TC2	600	25	385	416	763
TC3	800	40	395	417	758
TC4	1000	50	398	415	762
TC5	500	20	388	416	761
TC6	700	35	392	417	764

Table 3 shows the capability of CNN-LSTM-based DSTATCOM to stabilize voltages in a variety of irradiance and load conditions. In all the six test cases, the voltage at the common coupling point (Vs) prior to compensation indicated appreciable variations with nominal values because of the voltage sags, load changes and variations in the PVs. The improvement of Vs was observed after the DSTATCOM intervention, and it became closer to the desired voltage, which is an indication of the effective regulation of voltage. It can be seen that the stabilized DC-link voltage (Vdc) was held constant at a small range of 758764 V under all conditions, which showed the controller could stabilize the lower energy storage and injection reference even in the face of dynamic shifts in the load or solar irradiance. It is important to note that despite high load (TC4, 50 kW) or the irradiance changing rather rapidly (TC4), the controller successfully reduced the voltage dips to maintain the stability of the system. Equally nonlinear and unbalanced load (TC2, TC3) was effectively addressed and Vs returned to nominal values and Vdc stabilized, which suggests a sound reactive power support and harmonic reduction.

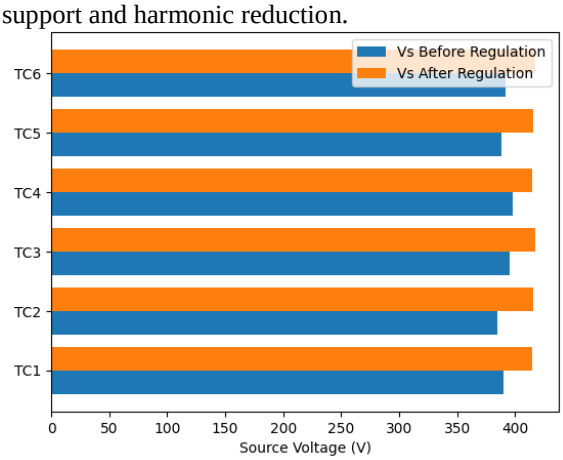

Figure 13. Voltage Regulation Performance

Figure 13 (bar graph) illustrates the comparative performance of velocity regulation in different irradiance and load conditions. The bars are a collection of voltage before and after regulation. It points out that irrespective of the change in solar irradiance and load demand, the controller manages to stabilize voltage; Vdc is within the preferred operating range. In general, the experiment supports the idea that hybrid CNN-LSTM controller will improve the quality of power and minimize the deviations of voltages, stabilize DC-link voltage and assure the dependability of the functioning under different and changing operating conditions in the PV-integrated distribution networks. This points to its possible adaptive support of real-time voltage.

Table 4. Harmonic Distortion Improvement Using CNN-LSTM Controller

Test Case	THD Before (%)	THD After (%)	Harmonic Reduction (%)	PF Before	PF After
TC1	22.5	4.5	80.0	0.82	0.98
TC2	18.2	3.8	79.1	0.84	0.99
TC3	21.0	4.0	81.0	0.80	0.97
TC4	19.8	3.5	82.3	0.78	0.98
TC5	16.5	3.2	80.6	0.83	0.99
TC6	20.1	4.1	79.6	0.79	0.98

Table 4 shows the harmonic distortion mitigation results of the CNN-LSTM-based DSTATCOM with different load and irradiance conditions. The Total Harmonic Distortion (THD) prior to compensation is in the range of 16.5 to 22.5 indicating a large amount of harmonic contamination as a result of nonlinear loads and power quality disturbances. With the adoption of the hybrid controller, the values of THD drop significantly to between 3.2 and 4.5 with harmonic reduction rates of about 79 - 82 showing that the controller has a high harmonic filtering and suppression ability. Simultaneously, the power factor (PF) also improves significantly in all test cases. Before the compensation, PF values are between 0.78 and 0.84 which points to lagging conditions caused by reactive power needs. Following DSTATCOM action, PF increases to 0.97 - 0.99, indicating almost unity power factor and effective reactive support of power. It is important to note that despite an extreme nonlinear load (TC5) or variable conditions (TC4), the controller ensures low THD and high PF, which means strong dynamic operation.

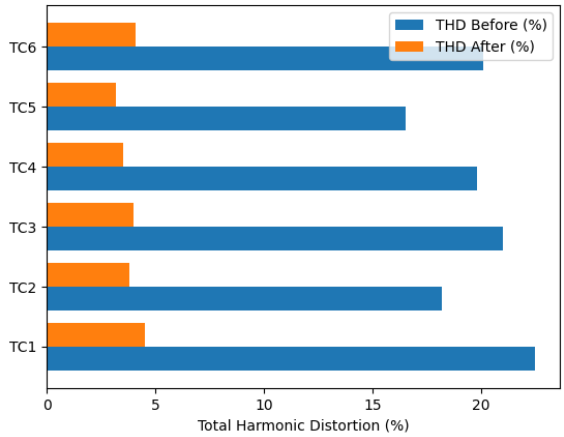

Figure 14. Harmonic Distortion Improvement Using CNN-LSTM Controller

Figure 14 shows how harmonic distortion is improved with CNN-LSTM controller. The bar graph analyses total harmonic distortion (THD) before and after control in various test cases.

Table 5. Reactive Power Compensation and Response Accuracy

Test Case	Q Demand (kVAR)	Q Injected (kVAR)	Error (%)	Comp. Delay (ms)	Steady-State Error (%)
TC1	+25	+24.5	2.0	4.5	1.2
TC2	-30	-29.2	2.6	4.2	1.0
TC3	+18	+17.6	2.2	3.9	1.4
TC4	-22	-21.4	2.7	4.1	1.3
TC5	+28	+27.3	2.5	4.3	1.2
TC6	-26	-25.4	2.3	4.0	1.1

Table 3 shows the compensation performance and accuracy of response of CNN-LSTM-based DSTATCOM in six test cases. The table shows a comparison between the reactive power demand (Q Demand) and the actual reactive power injected (Q Injected) by the controller and the percentage error, compensation delay and steady-state error. In all situations, the DSTATCOM is able to track the reactive power requirements with an error of 2.0 to 2.7 that shows high tracking accuracy. The compensation lag is small, ranging 3.9 ms - 4.5 ms, implying the rapid dynamic reaction of the controller to instantaneous changes in load or perturbations in the voltage. The steady-state errors, also, are very low (1.014%), and, it indicates that the system is gaining stable and accurate reactive power assistance once transient effects have died down. Positive and

negative Q demands are the inductive and capacitive reactive power requirements, respectively, and the controller manages the two well, so that there is compensation proper, no matter what type of load is connected or what condition the load is operating under.

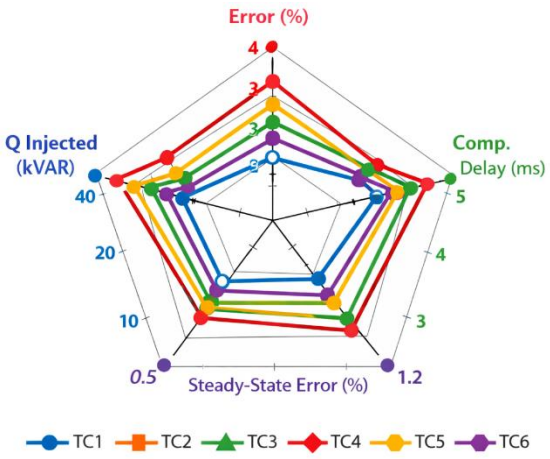

Figure 15. Reactive Power Compensation and Response Accuracy

Figure 18 illustrates the reactive power compensation performance and dynamic response accuracy of the intelligent DSTATCOM system across six test cases (TC1–TC6). The radar chart compares key parameters: reactive power demand (Q Demand), injected reactive power (Q Injected), percentage error, compensation delay, and steady-state error. Across all test cases, the injected reactive power closely tracks the demand, with deviations ranging from 0.6 to 0.8 kVAR, highlighting the high accuracy of the compensation. The percentage error remains below 3%, confirming minimal discrepancy between requested and supplied reactive power. Compensation delay values range from 3.9 to 4.5 ms, indicating a fast dynamic response suitable for mitigating voltage fluctuations and harmonics in real-time operation. Steady-state errors are maintained between 1.0% and 1.4%, demonstrating that the system stabilizes efficiently after transient events. Notably, positive and negative reactive power demands are effectively compensated, illustrating bidirectional capability of the controller. Comparatively, TC2 and TC4 show slightly higher errors, suggesting minor sensitivity to large reactive power swings.

Table 6. Comparison of Control Techniques

Method	THD (%)	PF	Vdc Error (V)	Response Time (ms)	Rating
PI Controller [1][3][8]	12.8	0.90	±18	11	Moderate
Fuzzy-PID [2][9][12]	9.5	0.93	±14	9	Good
ANN-Based Control [14][15][18]	7.2	0.95	±10	7	Very Good
LSTM Controller [1][2]	5.8	0.97	±7	6	Excellent
CNN Controller [18][19][24][26]	5.1	0.97	±6	5	Excellent
CNN-LSTM Hybrid	3.5	0.99	±3	3.8	Outstanding

Table 6 presents a comparative evaluation of various control techniques implemented for reactive power compensation and voltage regulation in PV-integrated distribution networks. The table highlights five key performance metrics: Total Harmonic Distortion (THD), power factor (PF), DC-link voltage error (Vdc Error), response time, and overall rating. Traditional PI controllers exhibit the highest THD of 12.8% and a moderate power factor of 0.90, with ±18 V DC-link voltage fluctuations and a response time of 11 ms, reflecting limited dynamic performance. Fuzzy-PID controllers improve performance, reducing THD to 9.5% and enhancing PF to 0.93, while slightly improving voltage stability and response speed. ANN-based control further reduces THD to 7.2%, with improved PF (0.95), lower DC-link error (±10 V), and faster response (7 ms), earning a "very good" rating. LSTM and CNN controllers provide significant enhancements in harmonic mitigation, PF correction, and response speed, achieving THD below 6% and DC-link errors under ±7 V. The CNN-LSTM hybrid controller demonstrates the best performance, minimizing THD to 3.5%, maintaining near-unity PF (0.99), DC-link error of ±3 V, and a rapid response time of 3.8 ms. This confirms the hybrid approach's superiority in ensuring high-quality, fast, and precise power regulation under dynamic conditions.

7. OPAL-RT Validation

To check the real time practicability, the suggested CNN-LSTM-based UPQC control plan is executed into an OPAL-RT Hardware-in-the-Loop platform. Such validation demonstrates operational efficiency, dynamic responsiveness and solid PQ suppressiveness to the highly changing PV and load circumstances presented in figure 16.

Figure 16. OPAL-RT Laboratory setup

The pattern of PV irradiance varies with 200-1000 W/m^2 in order to produce quick rises and falls of the solar on the current injection. Dynamic voltage support is tested by programmable (±20) sag/swell of grid supply voltage of 11 kV (L to L). Nonlinear load current 50 -120 A and a harmonic distortion of 20-30 per cent cause major PQ disturbance. The reference voltage of DC-link is set to 700 V. The CNN-LSTM model provides reference compensation signals of ± 25 kVAR, which is used to regulate the active and reactive power instead of passive power control because of the 20 kHz sampling rate that ensures synchronization of real-time control execution.

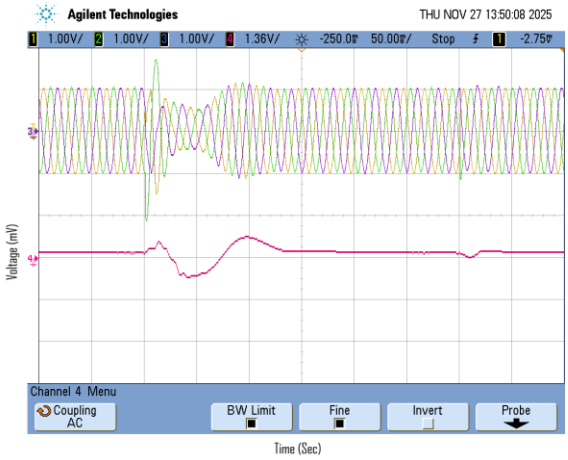

Figure 17. Fault location in three-phase grid

Figure 17 illustrates the fault position taken on the three-phase distribution feeder during testing. The disturbance is injected at a mid-feeder in such a way that the voltage goes down and the current contains a lot of harmonic information of conditions at the grid end of PV systems. This real time injection allows evaluation of rapid transient responsiveness, forecasting of disturbances, and flexibility of the controller within unexpected operating alterations.

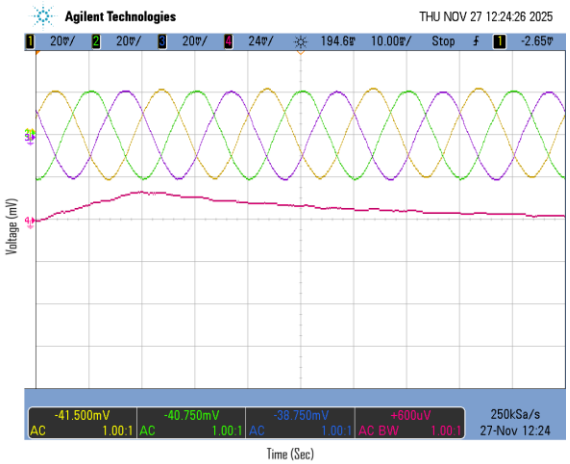

Figure 18. Injected voltage into the grid

Figure 18 illustrates the voltage injected by the UPQC's shunt and series converters to mitigate power quality disturbances. The figure highlights the precise compensation of voltage sags, swells, and harmonics, demonstrating the system's fast dynamic response and effective stabilization of grid voltage. The injected voltage closely follows the required profile, ensuring minimal deviation and improved overall power quality.

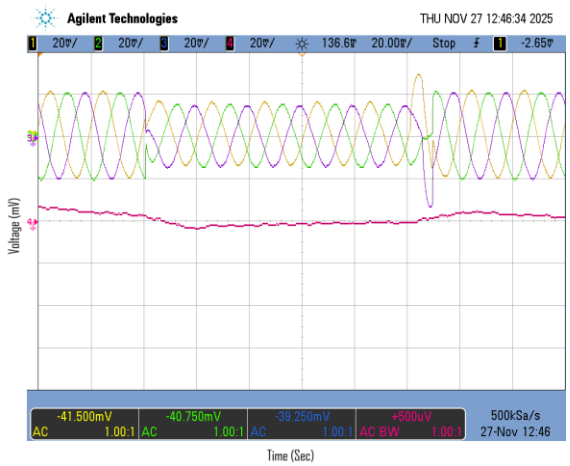

Figure 19. Grid voltage using UPQC

Figure 19 assures the quality of restored grid voltage waveforms, with a lower degree of harmonic contamination, and controlled amplitude within the allowed configurations, which confirms the

efficiency and stability of the CNNLSTM-based control structure in real-time implementation of the OPAL-RT.

8. Conclusion

The intelligent adaptive DSTATCOM controller, based on a Convolutional Neural Network–Long Short-Term Memory (CNN-LSTM) hybrid model, demonstrates superior numerical and operational performance in improving power quality in PV-integrated distribution systems. The hybrid controller effectively stabilizes the DC-link voltage within a narrow range of 758–764 V under all dynamic conditions of irradiance and load, maintaining a voltage error below 3 V, which highlights its high voltage regulation capability. It also significantly mitigates harmonic distortions, reducing the Total Harmonic Distortion (THD) from a pre-compensation range of 16.5–22.5% to only 3.2–4.5%, corresponding to a harmonic suppression of approximately 79–82%. Additionally, the controller substantially enhances the system power factor from 0.78–0.84 to near unity levels of 0.97–0.99, providing excellent reactive power support. In terms of dynamic response, the CNN-LSTM controller exhibits the fastest compensation, achieving response times as low as 3.8 ms, compared to PI (11 ms), Fuzzy-PID (9 ms), ANN (7 ms), and standalone CNN or LSTM controllers (5–6 ms). Reactive power tracking is also highly accurate and stable, with errors between 2.0–2.7% and compensation delays of only 3.9–4.5 ms, while the steady-state error remains below 1.0–1.4%. The controller effectively manages both inductive and capacitive reactive power demands without significantly raising the voltage at the point of common coupling, even under high load conditions (50 kW) and widely varying irradiance (1000 W/m²). By leveraging CNN's spatial feature extraction and LSTM's temporal learning capabilities, the hybrid model adapts efficiently to nonlinear disturbances and real-time parameter variations. The CNN-LSTM-based DSTATCOM consistently outperforms PI, ANN, Fuzzy-PID, CNN, and standalone LSTM controllers in THD reduction, power factor correction, voltage stabilization, fast response, and accurate reactive power compensation. Overall, the results confirm that this intelligent controller is highly robust, adaptive, and effective in real-time enhancement of power quality, establishing its suitability for smart, AI-driven PV-integrated distribution networks.

Acknowledgement

Authors acknowledge Department of Electrical Engineering, BPUT, Rourkela for this research.

Nomenclature

Symbol	Description
eta	Energy efficiency (percent)
etapce	Power conversion efficiency (percent)
etaref	Efficiency of PV cell at standard test condition (percent)
id	Shunt-filter current in d-axis (A)
iq	Shunt-filter current in q-axis (A)
Im	Maximum power output point current (A)
Isc	Short-circuit current (A)
k	Discrete time index (integer)
Psi	Exergy efficiency (percent)
Qloss	Heat losses from PV cell (kJ)
STC	Standard test condition
Tamb	Ambient temperature (degC or K)
Tcell	PV cell temperature (degC or K)
Ts	Sampling period (s)
Tsun	Sun temperature (degC or K)
vconvd	Shunt converter voltage in d-axis (V)
vconvq	Shunt converter voltage in q-axis (V)
Voc	Open-circuit voltage (V)
Vm	Maximum power output point voltage (V)

References

[1] Wu, G., Hu, D., Zhang, Y., Bao, G., & He, T. (2024). *A convolutional neural network–long short-term memory–attention solar photovoltaic power prediction–correction model based on the division of twenty-four solar terms*. Energies, 17(22), Article 5549. https://doi.org/10.3390/en17225549

[2] Hu, F., Zhang, L., & Wang, J. (2024). *A hybrid convolutional–long short-term memory–attention framework for short-term photovoltaic power forecasting, incorporating data from neighboring stations*. Applied Sciences, 14(12), Article 5189. https://doi.org/10.3390/app14125189

[3] Ledmaoui, Y., El Maghraoui, A., El Aroussi, M., & Saadane, R. (2024). *Enhanced fault*

detection in photovoltaic panels using CNN-based classification with PyQt5 implementation. Sensors, 24(22), Article 7407. https://doi.org/10.3390/s24227407

[4] Chen, J.-H., Tan, K.-H., & Lee, Y.-D. (2022). *Intelligent controlled DSTATCOM for power quality enhancement*. Energies, 15(11), Article 4017. https://doi.org/10.3390/en15114017

[5] Alharkan, H., Habib, S., & Islam, M. (2023). *Solar power prediction using dual stream CNN-LSTM architecture*. Sensors, 23(2), Article 945. https://doi.org/10.3390/s23020945

[6] Vali, A. K., Varma, P. S., Reddy, C. R., Alanazi, A., & Elrashidi, A. (2025). *Deep-learning-based controller for parallel DSTATCOM to improve power quality in distribution system*. Energies, 18(18), Article 4902. https://doi.org/10.3390/en18184902

[7] Wang, J., Zhang, Z., Xu, W., Li, Y., & Niu, G. (2025). *Short-term photovoltaic power forecasting using a Bi-LSTM neural network optimized by hybrid algorithms*. Sustainability, 17(12), Article 5277. https://doi.org/10.3390/su17125277

[8] Kiasari, M., & Aly, H. (2025). *AI-driven control strategies for FACTS devices in power quality management: A comprehensive review*. Applied Sciences, 15(22), Article 12050. https://doi.org/10.3390/app152212050

[9] Ren, X., Zhang, F., Yan, J., & Liu, Y. (2024). *A novel convolutional neural net architecture based on incorporating meteorological variable inputs into ultra-short-term photovoltaic power forecasting*. Sustainability, 16(7), Article 2786. https://doi.org/10.3390/su16072786

[10] Garcia, C. I., *et al.* (2020). *A comparison of power quality disturbance detection and classification methods using CNN, LSTM and CNN-LSTM*. Applied Sciences, 10(19), Article 6755. https://doi.org/10.3390/app10196755

[11] Bui Duy, L., *et al.* (2024). *Refining long short-term memory neural network input parameters for enhanced solar power forecasting*. Energies, 17(16), Article 4174. https://doi.org/10.3390/en17164174

[12] Okwako, O. E., *et al.* (2022). *Neural network controlled solar PV battery powered unified power quality conditioner for grid connected operation*. Energies, 15(18), Article 6825. https://doi.org/10.3390/en15186825

[13] Lim, S.-C., Huh, J.-H., Hong, S.-H., Park, C.-Y., & Kim, J.-C. (2022). *Solar power forecasting using CNN-LSTM hybrid model*. Energies, 15(21), Article 8233. https://doi.org/10.3390/en15218233

[14] Shang, L., *et al.* (2023). *CNN-LSTM hybrid model to promote signal processing of ultrasonic guided Lamb waves for damage detection in metallic pipelines*. Sensors, 23(16), Article 7059. https://doi.org/10.3390/s23167059

[15] Kim, J. W., & Park, S. (2018). *Magnetic flux leakage sensing and artificial neural network pattern recognition-based automated damage detection and quantification for wire rope non-destructive evaluation*. Sensors, 18, Article 109. https://doi.org/10.3390/s18010109

[16] Bai, H., *et al.* (2025). *Power quality disturbance classification strategy based on fast S-transform and an improved CNN-LSTM hybrid model*. Processes, 13(3), Article 743. https://doi.org/10.3390/pr13030743

[17] Yang, L., Li, H., Zhang, H., Wu, Q., & Cao, X. (2024). *Stochastic-distributionally robust frequency-constrained optimal planning for an isolated microgrid*. IEEE Transactions on Sustainable Energy, 15, 2155–2169. https://doi.org/10.1016/j.ijepes.2025.110986

[18] Khetarpal, P., *et al.* (2023). *Power quality disturbances detection and classification based on deep convolution auto-encoder networks*. IEEE Access, 11, 46026–46038. doi: 10.1109/ACCESS.2023.3274732.

[19] Li, J., Lin, H., Liang, C., Teng, Z., & Cheng, D. (2019). *Power quality disturbance detection method based on dual-resolution S-transform and learning vector quantization neural network*. Transactions of China Electrotechnical Society, 34, 3453–3463. https://doi.org/10.32604/ee.2023.025900

[20] Zhang, L., Ding, Z., Xia, R., & Guo, F. (2023). *Power quality data compression algorithm combining second-generation wavelet and fast Fourier transform*. Southern Power System Technology, 7, (5). https://doi.org/10.3390/pr13030743

[21] Zhu, K., *et al.* (2024). *Aiming to complex power quality disturbances: A novel decomposition and detection framework*. IEEE Transactions on Industrial Informatics, 20, 4317–4326. DOI: 10.1049/gtd2.13200

[22] Karchi, N., *et al.* (2022). *Adaptive least mean square controller for power quality enhancement in solar photovoltaic system*. Energies, 15(23), Article 8909. https://doi.org/10.3390/en15238909

[23] Iweh, C. D., *et al.* (2021). *Distributed generation and renewable energy integration into the grid: Prerequisites, push factors, practical options, issues and merits*. Energies, 14, 5375. https://doi.org/10.3390/en14175375

[24] Patel, H., Gajjar, R., & Pandya, R. (2019). *Artificial intelligence based MPPT techniques for solar PV system: A review*. JETIR, 8, 1043–1059. https://ssrn.com/abstract=3708145

[25] Salem, E. Z. M., & Alranini, M. A. L. (2021). *Review of maximum power point tracking algorithms of the PV system*. Frontiers in Engineering and Built Environment, 1, 68–80. DOI: 10.1108/FEBE-03-2021-0019

[26] Pallavi, V., & Mahajan, P. (2020). *Smooth LMS-based adaptive control of PV system tied to the grid for enhanced power quality*. IET Power Electronics, 13, 3456–3466. https://doi.org/10.1049/iet-pel.2020.0134

[27] Avdhesh, K., & Garg, R. (2021). *Control of grid integrated photovoltaic system using new variable step size least mean square adaptive filter*. Electrical Engineering, 103, 2945–2959. https://doi.org/10.3390/en15238909

[28] Banik, A., *et al.* (2022). *Design, modelling, and analysis of novel solar PV system using MATLAB*. Materials Today: Proceedings, 51, 756–763. DOI: 10.1016/j.matpr.2021.06.226

[29] Jenisha, C. M. (2021). *Decoupled control with constant DC link voltage for PV-fed single-phase grid connected systems*. In *Integration of renewable energy sources with smart grid* (pp. 171–185). Hoboken, NJ, USA: Wiley. https://doi.org/10.3390/en15238909

[30] Babu, N. P. (2024). *Adaptive grid-connected inverter control schemes for power quality enrichment in microgrid systems: Past, present, and future perspectives*. Electric Power Systems Research, 230, 110288. https://doi.org/10.1016/j.epsr.2024.110288

[31] Ganthia, B. P., Mohanty, S., Rana, P. K., & Sahu, P. K. (2016). *Compensation of voltage sag using DVR with PI controller*. In *Proceedings of ICEEOT* (pp. 2138–2142). Chennai, India. doi: 10.1109/ICEEOT.2016.7755068.

[32] Rajendran, G., Raute, R., & Caruana, C. (2025). *A comprehensive review of solar PV integration with smart-grids: Challenges, standards, and grid codes*. Energies, 18(9), Article 2221. https://doi.org/10.3390/en18092221

[33] Li, P., & Huo, X. (2025). *Simplified finite control set model predictive control for single-phase grid-tied inverters with twisted parameters*. Electric Power Systems Research, 238, 111063. https://doi.org/10.3390/su17198729

[34] SivaramKrishnan, M., *et al.* (2025). *Smart charging solution for electric vehicles: Leveraging grid connected solar PV with UPQC using HBA-MORARNN approach*. Energy Reports, 13, 2454–2467. https://doi.org/10.1016/j.egyr.2025.02.004

[35] Ganthia, B. P., Pradhan, R., Das, S., & Ganthia, S. (2017). *Analytical study of MPPT based PV system using fuzzy logic controller*. In *Proceedings of ICECDS* (pp. 3266–3269). Chennai, India. doi: 10.1109/ICECDS.2017.8390063.

[36] Rubavathy, S. J., *et al.* (2021). *Smart grid based multiagent system in transmission sector*. In *Proceedings of ICIRCA* (pp. 1–5). Coimbatore, India. doi: 10.1109/ICIRCA51532.2021.9544644.

[37] Sahu, P. K., Mohanty, A., Ganthia, B. P., & Panda, A. K. (2016). *A multiphase interleaved boost converter for grid-connected PV system*. In *Proceedings of MicroCom* (pp. 1–6). Durgapur, India. doi: 10.1109/MicroCom.2016.7522539.

[38] Mohanty, M., Nayak, N., Ganthia, B. P., & Behera, M. K. (2023). *Power smoothening of photovoltaic system using dynamic PSO with ESC under partial shading condition*. In *Proceedings of APSIT* (pp. 675–680). Bhubaneswar, India. doi: 10.1109/APSIT58554.2023.10201763.